Molecular Biology of the Cell
Vol. 9, 173–189, January 1998

Morphology of the Yeast Endocytic Pathway

Cristina Prescianotto-Baschong and Howard Riezman*

Biozentrum of the University of Basel, CH-4056 Basel, Switzerland

Submitted June 4, 1997; Accepted October 22, 1997
Monitoring Editor: David Boststein

Positively charged Nanogold (Nanoprobes, Stony Brook, NY) has been developed as a new marker to follow the endocytic pathway in yeast. Positively charged Nanogold binds extensively to the surface of yeast spheroplasts and is internalized in an energy-dependent manner. Internalization of gold is blocked in the *end3* mutant. During a time course of incubation of yeast spheroplasts with positively charged Nanogold at 15°C, the gold was detected sequentially in small vesicles, a peripheral, vesicular/tubular compartment that we designate as an early endosome, a multivesicular body corresponding to the late endosome near the vacuole, and in the vacuole. Experiments examining endocytosis in the *sec18* mutant showed an accumulation of positively charged Nanogold in approximately 30–50 nm diameter vesicles. These vesicles most likely represent the primary endocytic vesicles as no other intermediates were detected in the mutant cells, and they correspond in size to the first vesicles detected in wild-type spheroplasts at 15°C. These data lend strong support to the idea that the internalization step of endocytosis in yeast involves formation of small vesicles of uniform size from the plasma membrane.

INTRODUCTION

Yeast cells have been shown to internalize extracellular fluid, ligands bound to their receptors, and plasma membrane proteins. Internalization is time-, temperature-, and energy-dependent. Once internalized by endocytosis, most of the characterized molecules are transported to the vacuole where they are degraded. Transport to the vacuole has been proposed to pass through at least two membrane-bound compartments, which were identified by following endocytosis at low temperature (15°C), and have been termed early and late endosomes based upon the kinetics of appearance of radiolabeled, internalized pheromone in the biochemically separable organelles (Riezman, 1993; Singer-Krüger *et al.*, 1993). The occurrence and relative densities of these kinetically defined compartments show some similarity to mammalian systems (Gorvel *et al.*, 1991).

A genetic analysis of endocytosis has led to the identification of a number of genes that are required for at least three different steps in the pathway (Munn and Riezman, 1994; Munn *et al.*, 1995; Riezman *et al.*, 1996). Most of the mutants characterized thus far affect the internalization step of endocytosis. This step has been shown to be dependent upon actin (Kübler and Riezman, 1993) and a number of other gene products that affect actin function, including calmodulin (Kübler *et al.*, 1994), a type I myosin (Geli and Riezman, 1996), two proteins with sequence homology to amphiphysin (Munn *et al.*, 1995; Sivadon *et al.*, 1995), which seems to play a role in clathrin-dependent endocytosis in animal cells (Shupliakov *et al.*, 1997), and two proteins with Eps15 homology domains (Bénédetti *et al.*, 1994; Wong *et al.*, 1995; Wendland *et al.*, 1996). Eps15 binds the plasma membrane clathrin adaptor complex, AP-2, and localizes to the collar of clathrin-coated pits in animal cells (Benmerah *et al.*, 1995; Tebar *et al.*, 1996). Mutants in clathrin also show reduced endocytic internalization (Tan *et al.*, 1993). Remarkably, the internalization of several plasma membrane proteins seems to require their prior ubiquitination (Hein *et al.*, 1995; Galan *et al.*, 1996; Hicke and Riezman, 1996). This requirement may be conserved for certain endocytosed proteins in animal cells (Staub *et al.*, 1996; Strous *et al.*, 1996).

Transport of internalized ligand to and/or through the early endosome has been shown to be dependent upon Ypt51p and homologous proteins that are yeast

* Corresponding author: Biozentrum of the University of Basel, Klingelbergstrasse 70, CH-4056 Basel, Switzerland.

homologs of the small mammalian GTPase Rab5 (Singer-Krüger *et al.*, 1995), the *SEC18* gene product that is the yeast homologue of the *N*-ethylmaleimide-sensitive fusion protein and requires continuous input from the secretory pathway (Hicke *et al.*, 1997). Transport from late endosomes to the vacuole requires another small GTPase, Ypt7p, the yeast homologue of mammalian Rab7 (Schimmöller and Riezman, 1993).

While several molecular requirements for the yeast endocytic pathway have been identified (Munn and Riezman, 1994; Munn *et al.*, 1995) that suggest similarities to animal systems, relatively little work has been published concerning the morphology of the pathway. Recent studies have attempted to follow the endocytic pathway of the α-factor receptor by immunofluorescence and have identified the late endosome by immunogold localization of the receptor at the ultrastructural level (Hicke *et al.*, 1997). Recently, cationized ferritin has been used to identify apparent internalization structures that accumulate in an endocytic mutant (Wendland *et al.*, 1996).

To improve the morphological characterization of the yeast endocytic pathway, we have followed the internalization and intracellular targeting of positively charged Nanogold (Nanoprobes, Stony Brook, NY) by yeast spheroplasts. The positively charged Nanogold binds strongly to the cell surface and is internalized by an energy- and *END* gene-dependent mechanism. The Nanogold travels through small vesicles, a vesicular/tubular compartment, and a multivesicular body on its way to the vacuole. After internalization in a *sec18* mutant, the internalized Nanogold is found exclusively in 30- to 50-nm diameter vesicles, most likely the primary endocytic vesicles, consistent with a vesicular mechanism of transport to the early endosome. Development of this technique should allow a more detailed analysis of the endocytic pathway and the available endocytosis mutants.

MATERIALS AND METHODS

Yeast Strains, Growth Conditions, and Preparation of Spheroplasts

The wild-type strain used throughout these studies was RH144–3D (*MATa his4 leu2 ura3 bar1*). The following mutant strains were used: RH1995 (*MATa his4 leu2 ura3 bar1 end3::URA3*), and RH1737 (*MATa sec18–20 his4 leu2 ura3 bar1*).

All yeast strains were inoculated from saturated precultures and grown overnight in YPUAD medium (1% yeast extract, 2% peptone, 2% glucose, 40 mg/l uracil and adenine) to an OD_{600} of 0.7–1.0. The cells were collected by centrifugation and converted to spheroplasts (Kübler *et al.*, 1994) with some modifications. The cells were resuspended in one-half the original volume with 0.1 M Tris·HCl pH 9.0/10 mM 2-mercaptoethanol and incubated for 10 min at room temperature (RT). The cells were again collected by centrifugation and washed once with 10 mM Tris·HCl, pH 7.0/0.7 M sorbitol/5% glucose/0.5 × YPUAD and resuspended in the same solution to 1–2 × 10^9 cells/ml, and then incubated with recombinant lyticase until most of the cells were converted to spheroplasts. The spheroplast preparation was centrifuged for 20 min at 1500 × *g* at RT and washed twice by resuspension in 10 mM Tris·HCl, pH 7.0/0.7 M sorbitol/1% glucose/0.5 × SD medium containing the appropriate additional nutrients (Dulic *et al.*, 1991). The spheroplasts were resuspended in the last buffer to a concentration of 10^9 spheroplasts/ml.

Incubations with Positively Charged Nanogold and Analysis by Electron Microscopy

Spheroplasts were incubated with positively charged Nanogold with two basic protocols. Spheroplasts (1 ml) were either incubated with 5 nmol of positively charged Nanogold at 0°C for 15 min and then warmed up to the indicated temperature or were preincubated at the indicated temperature before addition of 5 nmol of positively charged Nanogold. When sodium azide and sodium fluoride (10 mM each) were used, they were included in the preincubation period. The spheroplasts were then incubated for various times at the indicated temperature before fixation by direct addition of formaldehyde and glutaraldehyde to final concentrations of 3 and 0.2%, respectively.

Spheroplasts were fixed for 2 h at RT or overnight at 4°C. After fixation, samples were washed three times with 50 mM HEPES, pH 7.0/3 mM KCl. The spheroplasts were then treated with 1% metaperiodate for 30 min to avoid problems in the embedding procedure due to the remaining cells that were not converted to spheroplasts (van Tuinen and Riezman, 1987). Dehydration, infiltration, and polymerization were done according to the protocol furnished with the LR GOLD resin (London Resin, London, England). Thin sections of about 50 nm were cut and mounted on nickel grids. The positively charged Nanogold was enhanced with HQ Silver (Nanoprobes) for 4 min as described by the manufacturer. Sections were then stained with 6% uranyl acetate for 10 min. The sections were examined with a Philips 400 electron microscope (Philips Electronic Instruments, Mahwah, NJ) at 80 kV.

Labeled structures were counted for the internalization experiment at 15°C from 20 independent labeled spheroplast profiles from the indicated time points by two different people. The total numbers from the 20 sections at each time point were averaged and an SD determined. Labeled vesicles, vesicular/tubular structures (early endosomes), spherical or ovoid structures (late endosomes), and vacuoles were counted.

Quantitation of endocytosis of positively charged Nanogold by *end3* spheroplasts and wild-type cells was performed by counting the number of gold particles revealed by the enhancement procedure that were on the cell surface and interior of five spheroplast sections. The total numbers were used to calculate the percentage of internalized positively charged Nanogold. The total number of gold particles counted was 4160 for wild-type spheroplasts and 4711 for *end3* mutant spheroplasts.

Vesicles, early endosomes, and late endosomes that were labeled with positively charged Nanogold were counted from 20 sections at each time point and temperature for *sec18* mutant spheroplasts. Nonpermissive temperature was 32°C, and permissive temperature was RT.

RESULTS

Positively Charged Nanogold Can Be Used as an Endocytic Marker

Wild-type yeast cells were grown overnight in rich medium, collected by centrifugation, and converted to spheroplasts in sorbitol-enriched growth medium. The spheroplasts were cooled on ice, and positively charged Nanogold was added and allowed to bind to the cell surface. After 15 min incubation on ice the

sample was warmed to RT and incubated for 30 min before fixation. The fixed spheroplasts were dehydrated and embedded, and thin sections were prepared. As the size of the positively charged Nanogold is too small to be seen well by conventional electron microscopy, the gold was enhanced using HQ Silver and visualized in a Philips 400 electron microscope. After incubation of spheroplasts at RT, substantial gold labeling as a rather fine dark precipitate could been seen inside the cells in the vacuole and in a number of other intracellular membrane-bounded structures, some of which resemble the previously described late endosome (Figure 1A) (Hicke *et al.*, 1997). The endocytic nature and specificity of the procedure were verified in several ways. Visualization of the positively charged Nanogold required enhancement because if this part of the procedure was left out, we found that no gold precipitate whatsoever was detected (our unpublished observations). Detection also required incubation with the positively charged Nanogold because enhancement performed on spheroplasts that were not incubated with gold showed only a low and characteristic background (Figure 1C). The background due to the enhancement procedure was somewhat variable and increased with the age of the enhancement solutions, but was distinguishable from the real signal resulting from enhancement of the positively charged Nanogold because the latter gave a finer precipitate (Figure 1A).

To test for energy dependence of the internalization of the positively charged Nanogold, we incubated spheroplasts under the same conditions as above, but with addition of sodium azide and sodium fluoride to block ATP production from glycolysis and oxidative phosphorylation. Under these conditions, heavy labeling was seen on the surface of the spheroplasts, but no internalization of positively charged Nanogold occurred, showing the energy dependence of this process. Some cell surface invaginations could be seen under these conditions (Figure 1D), but we do not know whether these structures are related to *bona fide* endocytic internalization structures.

Due to the relatively large size of the positively charged Nanogold (1.4 nm diameter), it is most likely that the internalization occurred by endocytosis. To verify this, *end3* mutant spheroplasts, which are defective for the internalization of both fluid phase and membrane-bound markers (Raths *et al.*, 1993), were incubated as described above for the wild-type spheroplasts in the presence of sorbitol-enriched growth medium and positively charged Nanogold. The *end3*Δ mutant is defective for endocytosis at all temperatures (Bénédetti *et al*., 1994). Even after 30 min incubation at RT, virtually all of the positively charged Nanogold was found at the surface of the spheroplasts. This difference was quantified by counting the number of particles that were seen on the surface and interior of five complete sections of spheroplast profiles of approximately equal size. For wild-type spheroplasts, 11.5% of the gold was internal after 30 min incubation, whereas for *end3* spheroplasts this amount was only 0.4% (Figure 2). We conclude from these experiments that positively charged Nanogold can be used as an endocytic marker at the ultrastructural level because it is internalized by an energy-dependent, *END* gene-dependent mechanism and is delivered to the vacuole, as are other known markers of endocytosis, such as α-factor (Singer and Riezman, 1990), the pheromone receptors (Davis *et al.*, 1993; Schandel and Jenness, 1994), and several transporters (Berkower *et al.*, 1994; Volland *et al.*, 1994; Egner *et al.*, 1995; Lai *et al.*, 1995).

Ultrastructure of Endocytic Intermediates

To characterize intermediates in the endocytic pathway of yeast, we allowed the positively charged Nanogold to bind to yeast spheroplasts at 0°C, and then raised the temperature to 15°C, a temperature at which the transport rate through endosomes is differentially decreased compared with internalization (Singer and Riezman, 1990), and incubated for various times before fixation, embedding, and visualization of the surface-bound and internalized positively charged Nanogold. After incubation on ice the positively charged Nanogold was seen on the cell surface and in shallow plasma membrane invaginations, but not inside the cells (Figure 3A). After an 8-min incubation at 15°C, positively charged Nanogold was still found on the cell surface, sometimes in deeper cell surface invaginations (Figure 3B), but also seen inside the spheroplasts, where mainly small (~30–50 nm diameter) vesicular structures were labeled (Figure 3C). These vesicles were the most abundantly labeled structure at this time (Figure 4).

After a 12-min incubation at 15°C, cell surface and vesicle labeling was still seen, but labeling of a vesicular/tubular-like structure became easily apparent (Figure 4, A and B). This structure was seen as early as after 8 min at 15°C, but labeled profiles with this structure increased greatly by 12 min (Figure 4). It was not possible to determine with our technique whether the vesicle profiles were physically connected, but the structure was often seen with a horseshoe-like shape and extended over 250–300 nm, suggesting either continuity or binding of the vesicles to an underlying framework. Indeed, labeling of both the tubular and vesicular parts of this structure was evident, with somewhat more labeling of the tubular components (Figure 6). Labeling of this structure was still apparent after 20 min of incubation, which is to be expected for an early endocytic intermediate because internalization of positively charged Nanogold probably occurred continuously during the incubation. Based on

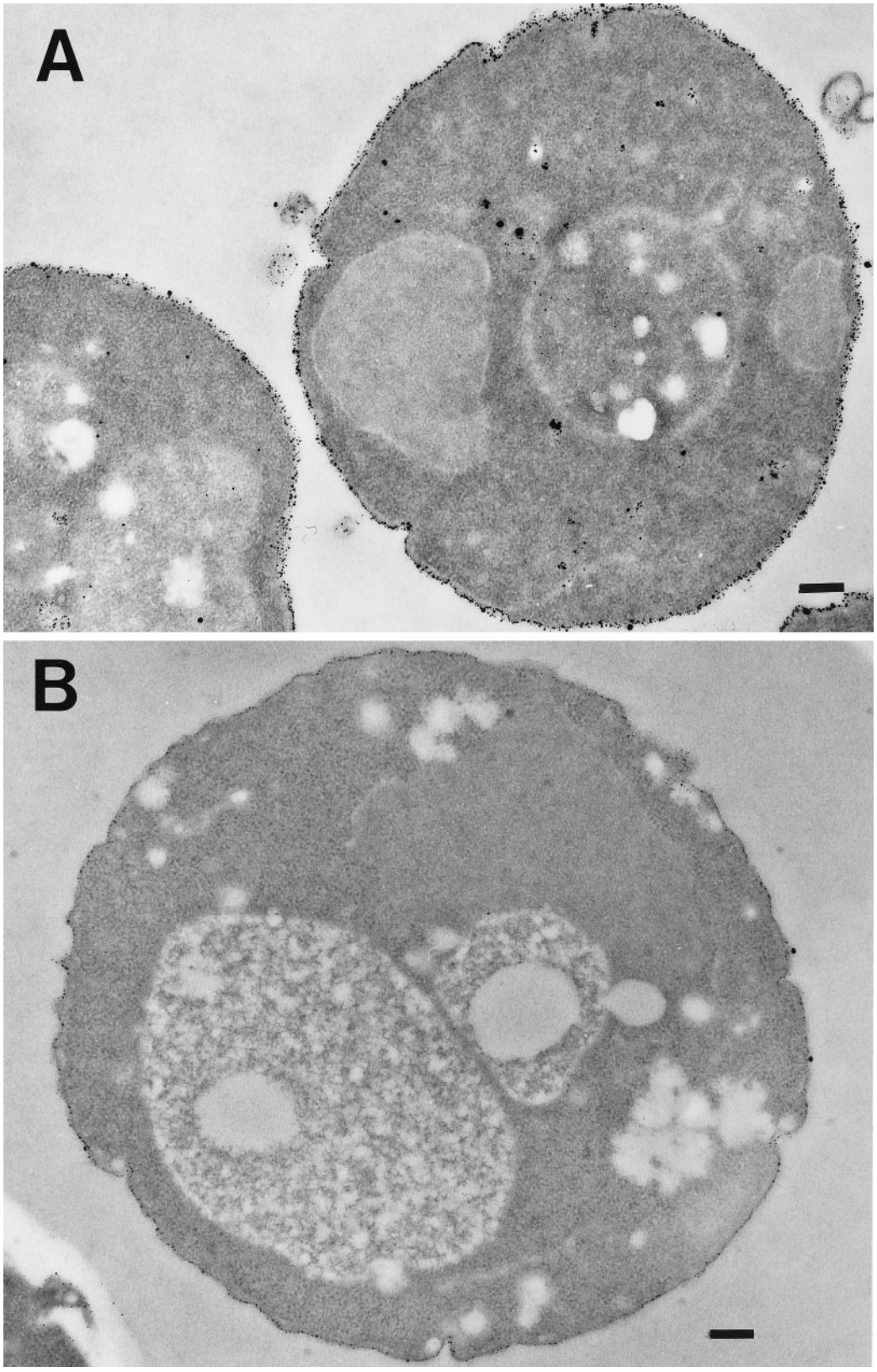

Figure 1 C and D (facing page).

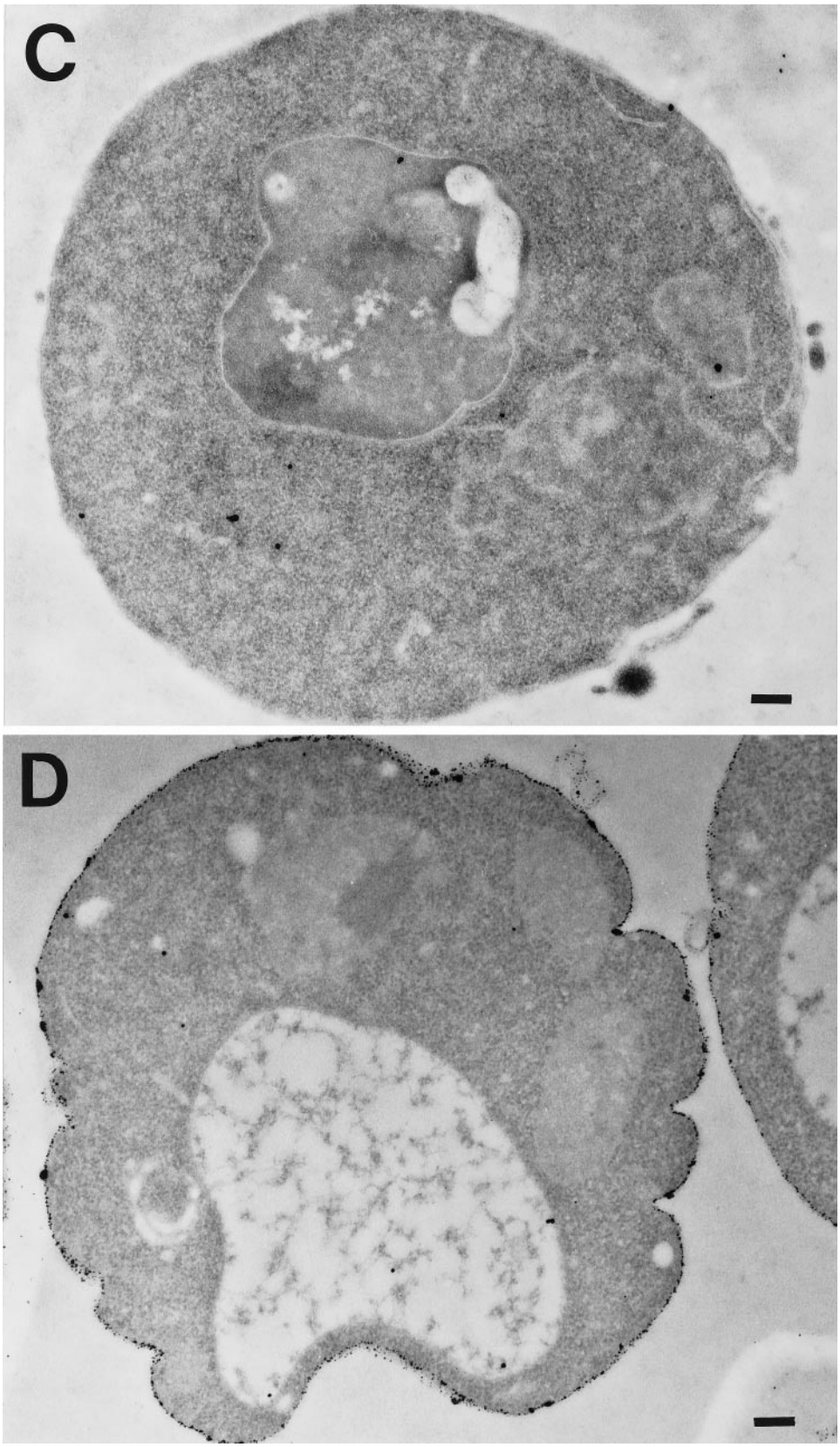

Figure 1. (cont.) Positively charged Nanogold can be used as an endocytic marker. Wild-type and *end3* mutant strains were grown overnight, converted to spheroplasts, and incubated under various conditions on ice for 15 min followed by a 30-min incubation at RT. The samples were fixed and embedded and thin sections were cut. (A) Sections from wild-type cells incubated with positively charged Nanogold were enhanced with HQ Silver. (B) Sections from *end3* mutant cells incubated with positively charged Nanogold and enhanced. (C) Sections from wild-type cells incubated in the absence of positively charged Nanogold, but enhanced. (D) Sections from wild-type cells incubated with positively charged Nanogold in the presence of NaN_3 and NaF and enhanced. The cells were visualized in the electron microscope as described in MATERIALS AND METHODS. Bar, 200 nm.

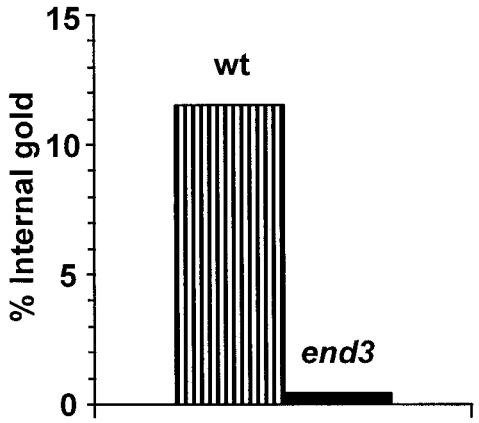

Figure 2. Quantitation of internalization by *end3* spheroplasts. Positively charged Nanogold was incubated with wild-type and *end3* spheroplasts as described in Figure 1, A and B. Gold particles were counted for five sections each on the plasma membrane and over the cell interior. The percentage of internal gold particles was calculated and plotted. The total number of cell surface particles counted was 3680 for wild-type spheroplasts and 4692 for *end3* spheroplasts.

the time course of appearance of label in these structures, they may represent the morphological equivalent of biochemically defined early endosomes, through which α-factor passes on its way to the vacuole (Singer-Krüger *et al.*, 1993). These structures were often located peripherally in the cell, consistent with previous immunofluorescence studies of the α-factor receptor after short times of internalization and after a block in the *sec12* mutant (Hicke *et al.*, 1997).

After 20 min, and more evidently after 90 min, all of the earlier structures were still seen, but another structure resembling the late endosome described previously (Hicke *et al.*, 1997) became abundantly (Figure 5C and D; Figure 7) and frequently (Figure 4) labeled. This is a multivesicular structure containing internal membranes and corresponds in its morphology and location to the previously defined late endosome (Figure 8) (Hicke *et al.*, 1997). The late endosomal compartment was relatively large, frequently spherical or oval in shape and approximately 200 nm across (Figure 8). It was most often found near the vacuole. The interior of the late endosome contained an electron-dense reticulum, most likely internal membranes. Most, if not all, of the gold labeling occurs on these internal membranes, suggesting that the internal membranes of this structure are derived from the plasma membrane.

In some cases, at this late time point, some vacuolar labeling was also detected. Vacuolar labeling was always less dense than that found in the late endosomes. This was expected because delivery of endocytic markers to the vacuole is greatly reduced at 15°C (Singer and Riezman, 1990) and because the volume of a late endosome is less than 1% that of the vacuole. We suggest from these studies that the positively charged Nanogold follows the following endocytic pathway; cell surface → vesicles → vesicular/tubular structure (early endosome) → multivesicular endosome (late endosome) → vacuole. This is likely to be similar to the endocytic pathway that α-factor and its receptor follow (Singer-Krüger *et al.*, 1993; Hicke *et al.*, 1997).

Small Endocytic Vesicles Accumulate in the sec18 Mutant

One particular feature of the yeast endocytic pathway is that the internalization step is blocked partially by mutants in clathrin (Tan *et al.*, 1993) and completely by mutants in actin and proteins that affect actin structure (Kübler and Riezman, 1993; Riezman *et al.*, 1996). Clathrin-coated vesicles detected by electron microscopy vary in diameter from approximately 60 to 100 nm (Stoorvogel *et al.*, 1996), including the coat. An intact actin network is also required for internalization through caveolae (Parton *et al.*, 1994). Vesicles formed through this pathway have an apparent size of 60–70 nm in diameter. Phagocytosis, which requires actin as well, results in the internalization of much larger structures of variable size. Therefore, we wanted to determine the size and uniformity of the primary endocytic intermediates in yeast. To do this we used a mutant that could block their fusion, but still permit their formation.

Sec18p is the yeast homolog of the N-ethylmaleimide-sensitive fusion protein that is required for many vesicle fusion events in yeast in the secretory pathway (Graham and Emr, 1991) and is implicated in homotypic fusion of vacuoles (Haas and Wickner, 1996), and the *sec18* mutation confers the earliest known postinternalization block in the endocytic pathway (Hicke *et al.*, 1997). We reasoned, therefore, that the *sec18* mutation is likely to block fusion of the primary endocytic vesicles with their target. Therefore, we performed an internalization experiment using positively charged Nanogold in the *sec18* mutant at nonpermissive temperature. Spheroplasts from wild-type or *sec18* mutant cells were shifted to 32°C for 10 min to inactivate mutant Sec18p, positively charged Nanogold was added, and the spheroplasts were incubated for a further 30 min and visualized by electron microscopy as described above. In wild-type cells, all of the above described compartments, including the vacuole (Figure 9A), were labeled, showing that the internalization protocol works at 32°C. Most of the positively charged Nanogold remained at the cell surface under these conditions in the *sec18* mutant (Figure 9B). The *sec18* spheroplasts accumulated a number of small vesicles of homogeneous size of which only a subset were labeled with positively charged Nanogold, consistent with the requirement for Sec18p for numerous

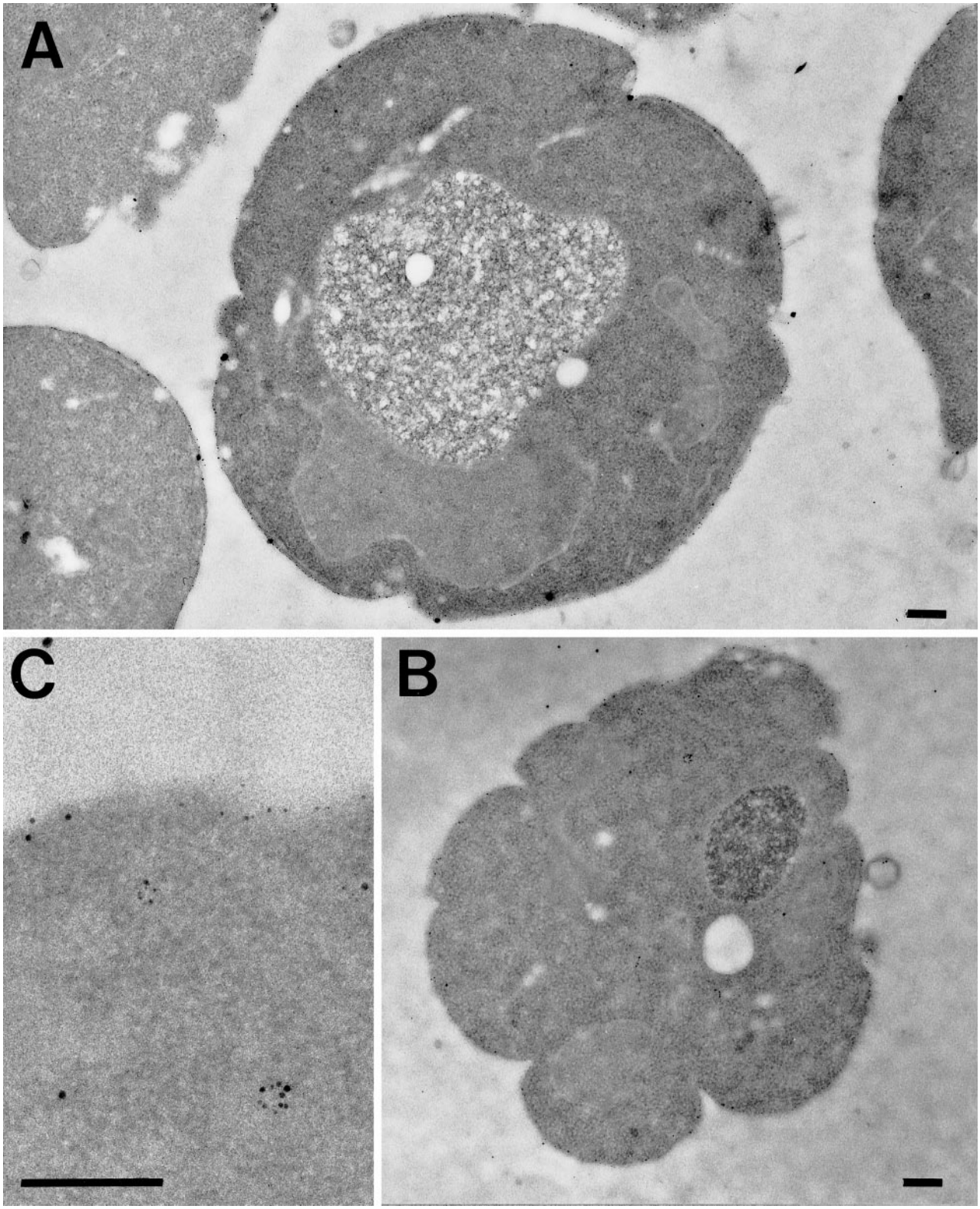

Figure 3. Endocytosis at early time points. Wild-type cells were grown overnight, converted to spheroplasts, and incubated with positively charged Nanogold on ice for 15 min (A) and subsequently warmed up to 15°C for 8 min (B and C). The spheroplasts were prepared for electron microscopy and visualized as in Figure 1A. Bar, 200 nm.

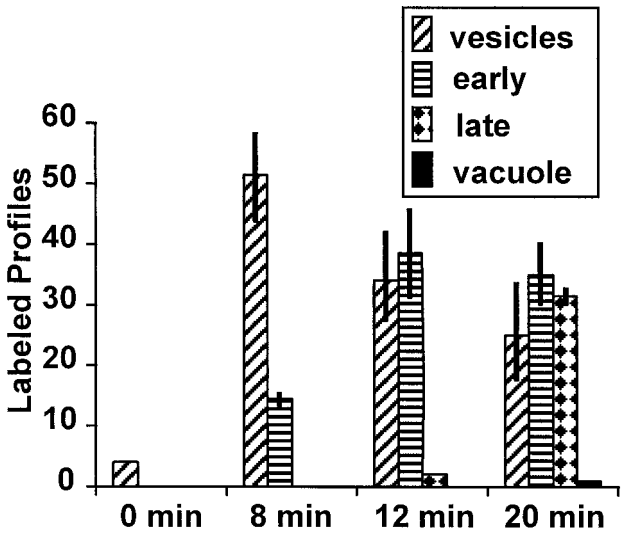

Figure 4. Quantitation of labeled profiles. Wild-type cells were grown overnight, converted to spheroplasts, and incubated with positively charged Nanogold on ice for 15 min and subsequently warmed up to 15°C for 0, 8, 12, or 20 min. Labeled vesicles, vesicular/tubular structures (early), oval or spherical structures (late), or vacuoles were counted. The numbers represent an average of two independent countings of the total number of labeled profiles over 20 spheroplast profiles.

intracellular membrane fusion events. The internalized, positively charged Nanogold was found exclusively in small vesicles of approximately 30–50 nm diameter (Figures 9C and 11) that seem to be similar or identical to those detected at early time points at 15°C (Figure 3C). No positively charged Nanogold was seen in structures resembling the early or late endosomes described above. To quantify the endocytic block and show that these vesicles accumulate due to the block imposed by the *sec18* mutation, we performed positively charged Nanogold internalization experiments for various times at permissive temperature (RT) and nonpermissive temperature (32°C) in the *sec18* mutant spheroplasts. At RT, vesicles accumulated with time, but this accumulation peaked at the 10-min time point. Both early and late endosomes were detected at the later time points (Figure 10). At nonpermissive temperature, only vesicles were seen, and they accumulated with time throughout the experiment. In addition, appearance of the vesicles in *sec18* spheroplasts containing positively charged Nanogold was dependent upon endocytosis because it was completely blocked in an *end3 sec18* double mutant (our unpublished observations). Therefore, we suggest that the *sec18* mutation blocks fusion of the primary endocytic vesicles in yeast and that the latter are of a relatively small and uniform size.

DISCUSSION

In this paper we have developed the use of positively charged Nanogold to follow the endocytic pathway in yeast at the ultrastructural level. Positively charged Nanogold fulfills all of the criteria for an endocytic marker. Its internalization is time-, temperature-, and energy-dependent, and it is only found on the cell surface or within membrane-bound internal compartments. Its internalization is greater than 20-fold reduced in the *end3* mutant, which has previously been shown to be required for the internalization of a number of endocytic markers, including a fluid phase marker, lucifer yellow CH (Riezman, 1985), a membrane phase marker, FM4–64 (Vida and Emr, 1995; Wendland *et al.*, 1996), as well as several specific markers, including α-factor, pheromone receptors, and permeases (Davis *et al.*, 1993; Raths *et al.*, 1993; Volland *et al.*, 1994; Lai *et al.*, 1995). Positively charged Nanogold is a nonspecific probe that has several advantages as a marker for absorptive endocytosis. It binds strongly and evenly to the surface of spheroplasts, and it can be used to generate an electron-dense aggregate that can be visualized in the electron microscope even though it is, itself, relatively small, and cannot be degraded, allowing its visualization throughout the endocytic pathway, including after delivery to the vacuole. Cationized ferritin has been used to follow endocytosis in yeast spheroplasts (Wendland *et al.*, 1996). This marker is also electron dense; however, it is much larger than positively charged Nanogold and is subject to degradation, introducing another variable into the experimental conditions. Therefore, the use of positively charged Nanogold should be of general use in the analysis of endocytic compartments and mutants.

The use of positively charged Nanogold and mutant cells has allowed us to visualize and confirm the existence of distinct organelles along the endocytic pathway, including primary endocytic vesicles, a vesicular/tubular structure that we term an early endosome, late endosomes, and vacuoles. As in animal cells, there are two biochemically and morphologically distinct organelles in the endocytic pathway in addition to the primary endocytic vesicles. Overall, it is remarkable that the endocytic organelles from yeast appear quite similar to those described for endocytic organelles in animal cells. The late endosome, which has been visualized previously using antibodies to the α-factor receptor (Hicke *et al.*, 1997), is a multivesicular compartment similar to that found for animal cells (McDowall *et al.*, 1989). The organelle is rather large, being one of the more conspicuous organelles in yeast after the nucleus and vacuole. After fixation, embedding, and visualization, the lumen of the organelle contains internal membranes but is not very electron dense, consistent with its distribution in low-density fractions in equilibrium density gradients (Singer-Krüger *et al.*,

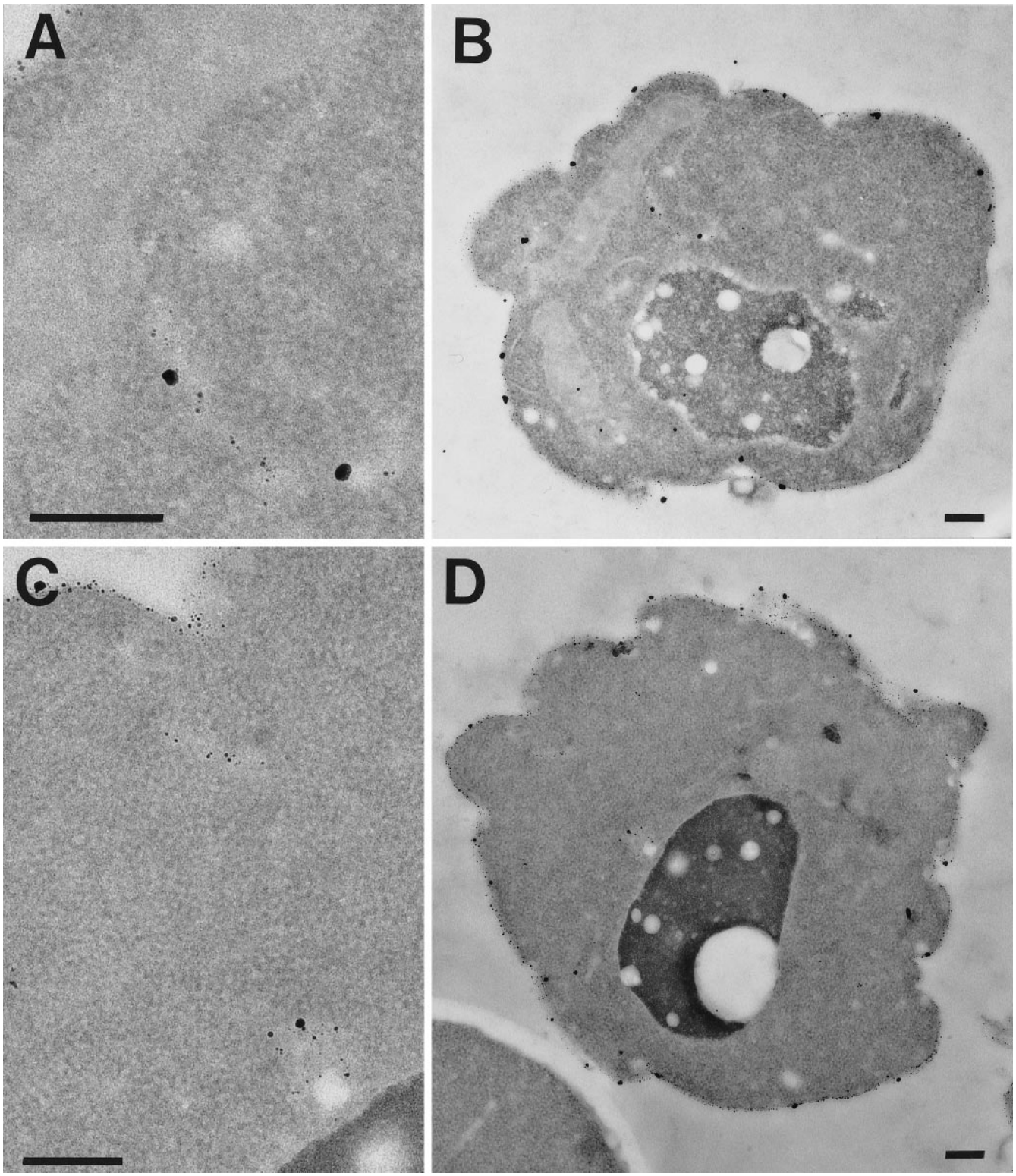

Figure 5. Early and late endocytic structures. Wild-type cells were grown overnight, converted to spheroplasts, and incubated with positively charged Nanogold on ice for 15 min and subsequently warmed up to 15°C for 12 min (A and B) or 20 min (C and D). The spheroplasts were prepared for electron microscopy and visualized as in Figure 1A. Bar, 200 nm.

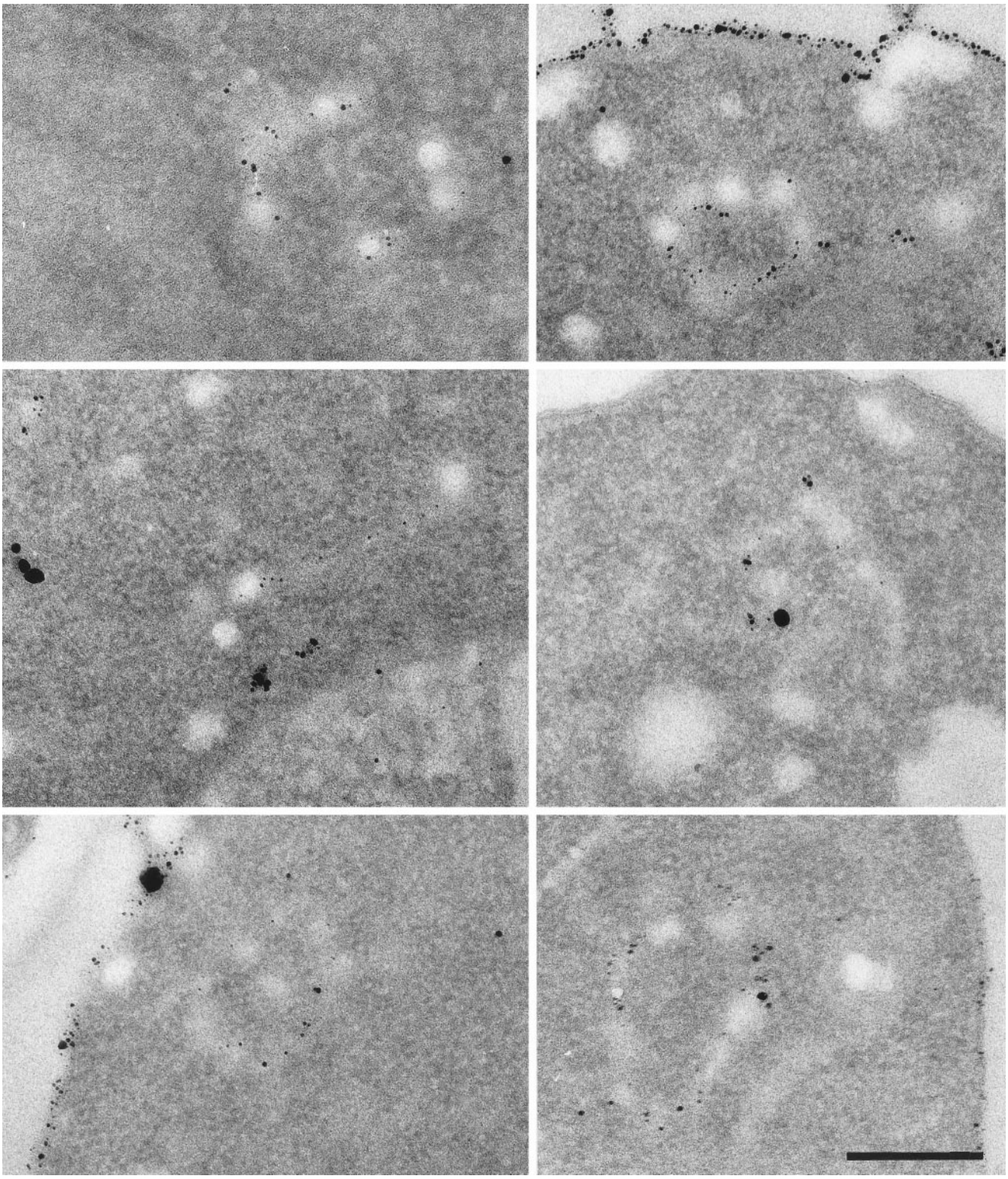

Figure 6. Early endosome profiles. Early endosomal profiles were taken from wild-type cells incubated and treated as in Figure 5. Bar, 200 nm.

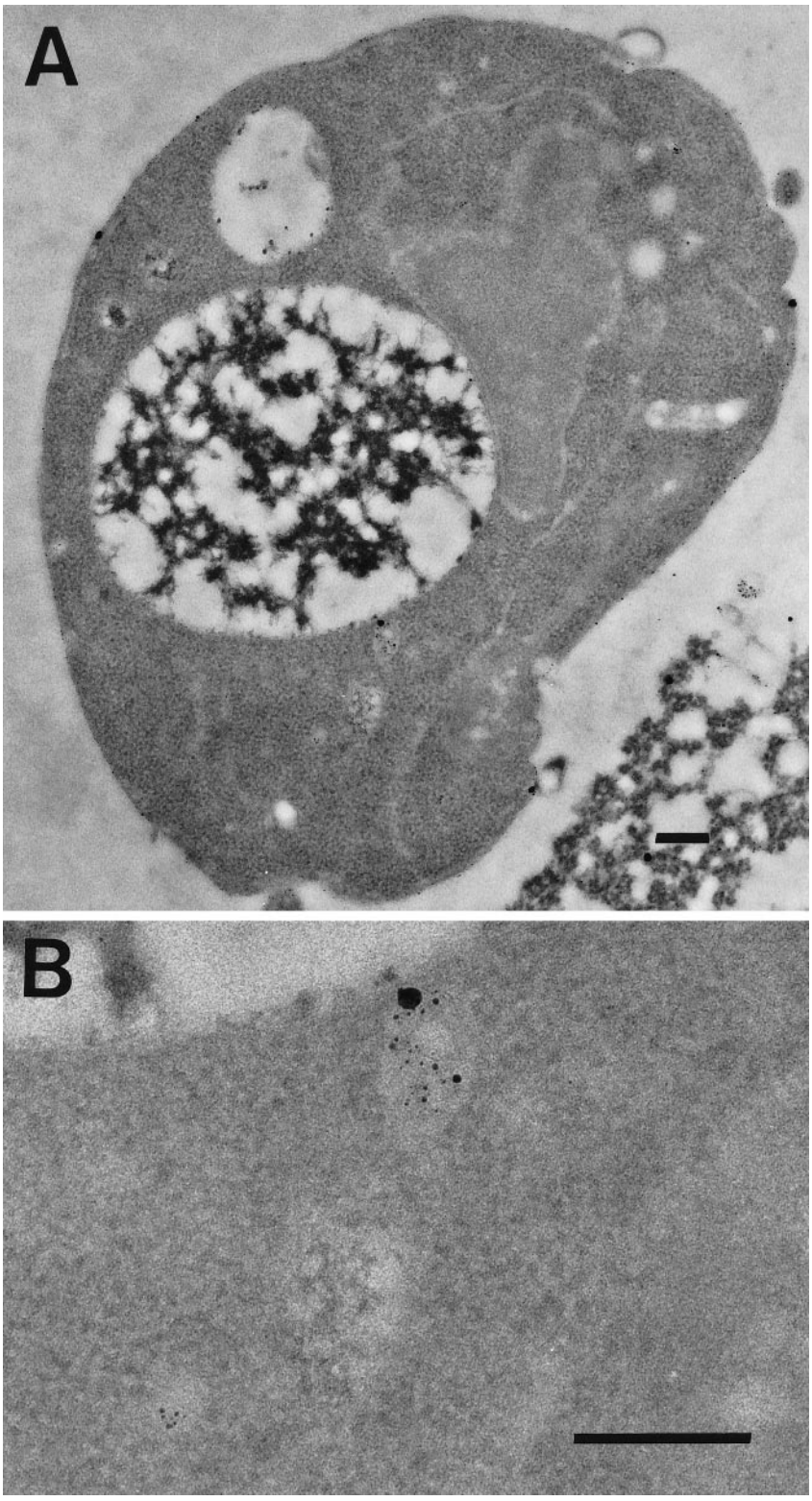

Figure 7. Late endocytic structures. Wild-type cells were grown overnight, converted to spheroplasts, and incubated with positively charged Nanogold on ice for 15 min and subsequently warmed up to 15°C for 90 min. The spheroplasts were prepared for electron microscopy and visualized as for Figure 1A. Bar, 200 nm.

1993). The late endosome is found most frequently, but not exclusively, close to the vacuole, and profiles can sometimes be seen where the late endosome may be fusing with the vacuole, but further analysis will be

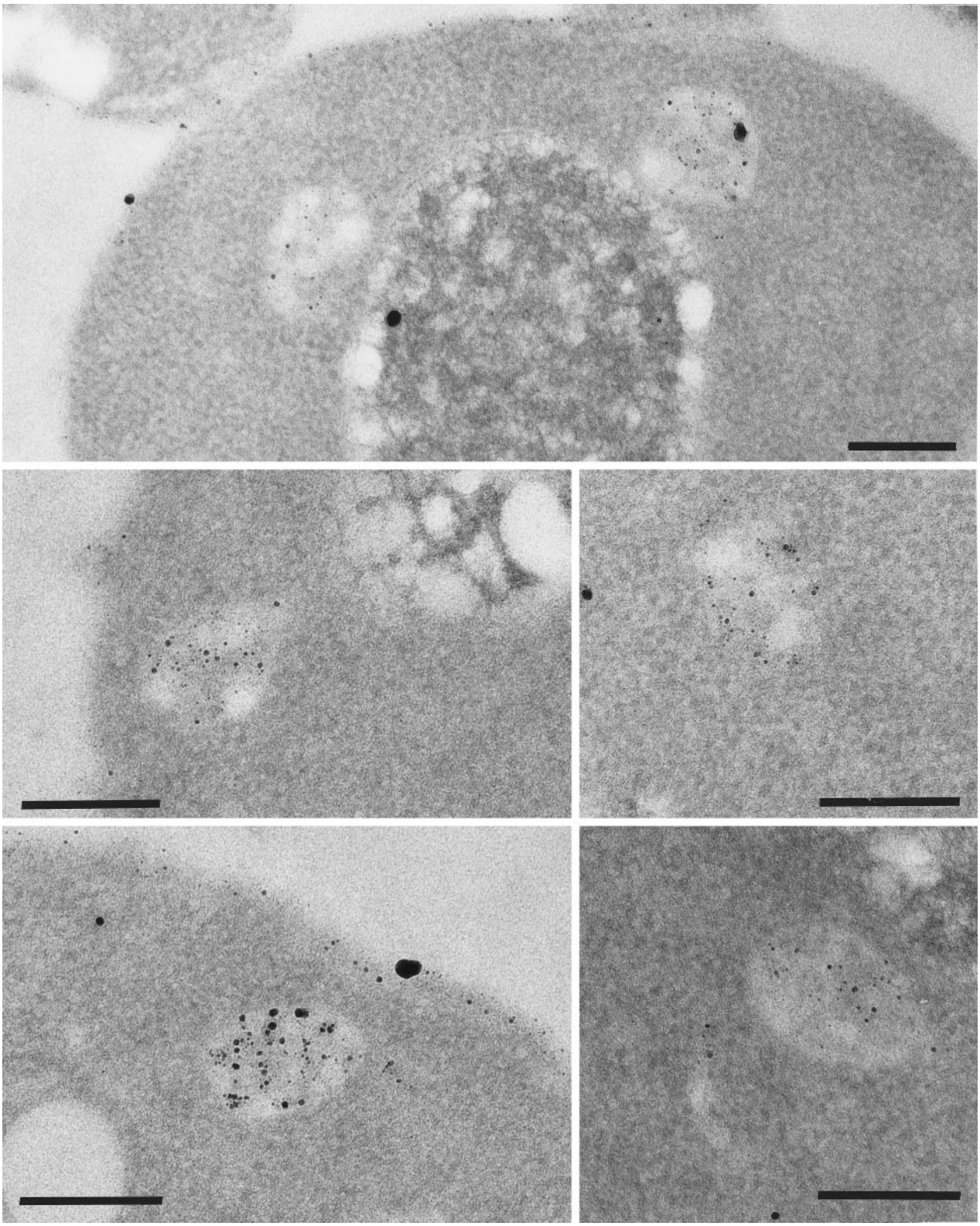

Figure 8. Late endosome profiles. Late endosome profiles were taken from wild-type cells treated as in Figure 5, C and D, or Figure 7. Bar, 200 nm.

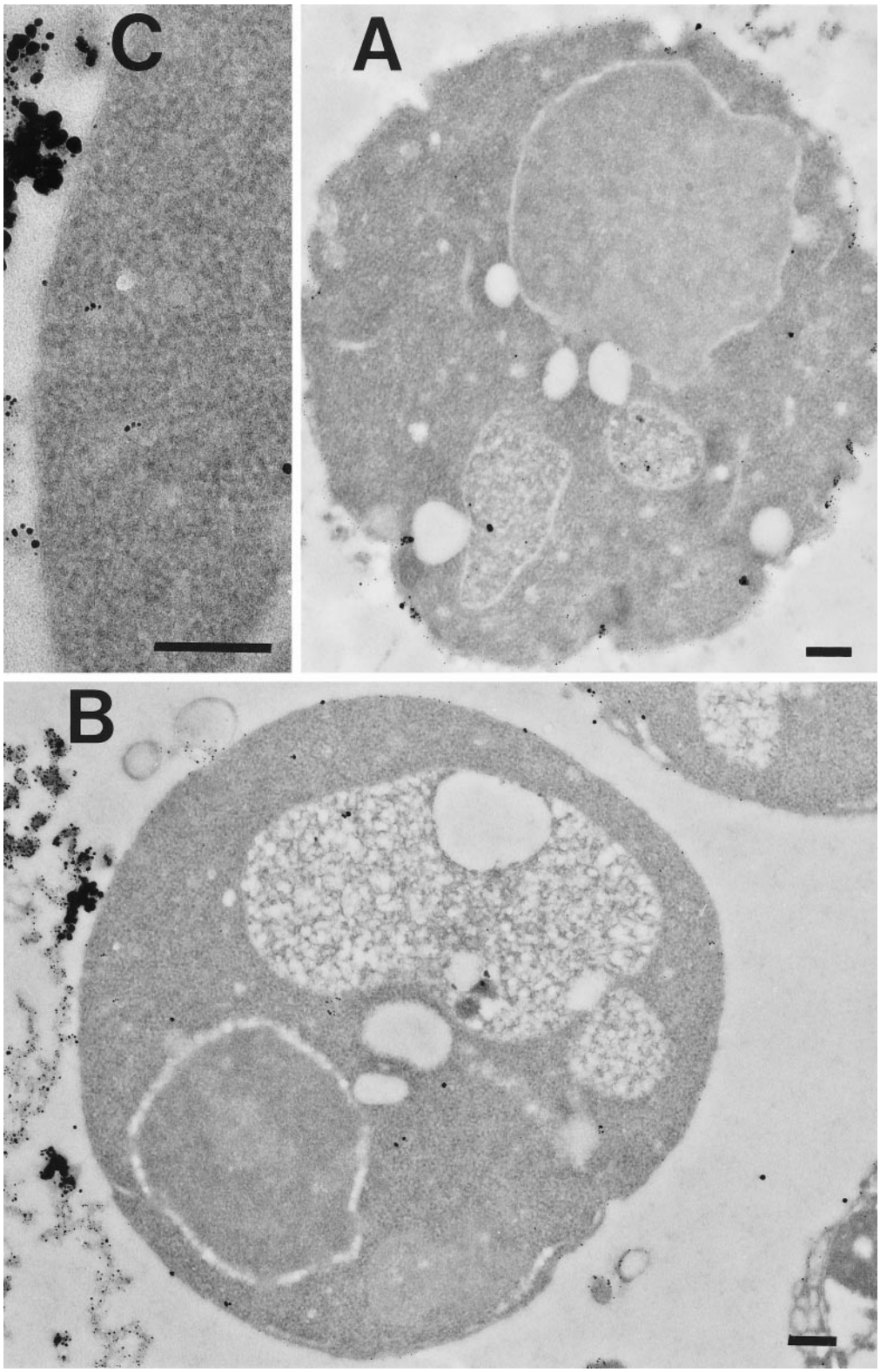

Figure 9. Small endocytic vesicles are seen in *sec18* spheroplasts. Wild-type (A) or *sec18* (B and C) cells were grown overnight, converted to spheroplasts, preincubated at 32°C for 10 min, and then incubated with positively charged Nanogold at 32°C for 30 min. The spheroplasts were prepared for electron microscopy and visualized as for Figure 1A. Bar, 200 nm.

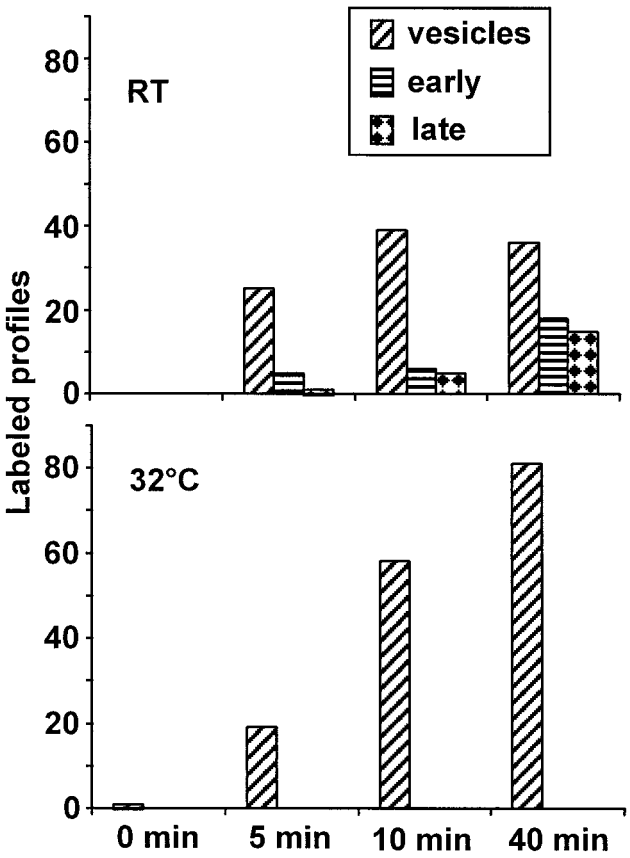

Figure 10. Small endocytic vesicles accumulate in *sec18* spheroplasts. Mutant (*sec18*) cells were grown overnight at 24°C, converted to spheroplasts, and incubated with positively charged Nanogold on ice for 15 min and subsequently warmed up to RT or nonpermissive temperature (32°C) for 0, 5, 10, or 40 min. Labeled vesicles, vesicular/tubular structures (early), and oval or spherical structures (late) were counted from 20 spheroplast sections at each time point and temperature.

necessary to address this point. It is interesting to note that most of the labeling was found on the internal structures of the late endosome, suggesting that the gold bound to plasma membrane molecules and early endosomes finds it way into the interior of this organelle. We cannot be certain, however, that these membranes are really internal. We cannot rule out that they are the result of multiple infoldings of the outer membrane of the structure, even though we did not detect any such infoldings in the multiple structures we examined.

At early time points of incubation with positively charged Nanogold at 15°C we could detect a labeled vesicular/tubular organelle. The low-temperature incubations allowed us to demonstrate that appearance of positively charged Nanogold in this structure preceded its appearance in the late endosome. This structure is not generated due to the low temperature incubations because it was also easily seen after internalization experiments at 30°C (our unpublished observations) and 32°C (Figure 9). This structure may be one of the morphological counterparts of biochemically defined early endosomes (Singer-Krüger *et al.*, 1993) because the structure is labeled early during time course incubations and is found mainly in the cell periphery in accordance with immunofluorescence studies (Hicke *et al.*, 1997). This structure resembles early endosomes from animal cells. In animal cells early endosomes have been postulated to be an interconnected structure with tubular and vesicular components (Hopkins *et al.*, 1990; Stoorvogel *et al.*, 1996). The vesicular components in animal cells are sometimes coated with clathrin (Stoorvogel *et al.*, 1996). Our early endosomal profiles could be very similar because we found both tubular and vesicular structures that were consistently associated with each other. Even if these components are not actually interconnected, there must be some underlying structure because the profiles seen are fairly distinct and well ordered. The gold labeling of these structures was found in both the tubular and vesicular parts but was more often associated with the tubular components. Some of the vesicular profiles were clearly unlabeled. This would be expected if some of the vesicular profiles resulted from incoming vesicles from the secretory pathway, e.g., from the trans-Golgi. Endocytic traffic from early to late endosomes requires a continuous input from the secretory pathway (Hicke *et al.*, 1997); therefore, one would expect such incoming traffic.

Putative Primary Endocytic Vesicles

Putative primary endocytic vesicles were visualized with the aid of the *sec18* mutant. In *sec18* cells, only small uniform vesicles of approximately 30–50 nm diameter were seen labeled with positively charged Nanogold at nonpermissive temperature. These vesicles were similar in size to other vesicles that accumulated in the *sec18* mutant (Figure 11) (Kaiser and Schekman, 1990). Several arguments suggest that these are primary endocytic vesicles. First, these were the only labeled structures that we detected in *sec18* spheroplasts at nonpermissive temperature, and they accumulated with time at nonpermissive temperature in the mutant spheroplasts. In wild-type cells at the same temperature all of the above described endocytic structures were labeled efficiently. If the positively charged Nanogold had reached the early endosome in the *sec18* spheroplasts we would have detected it as we did in wild-type cells after similar incubation periods. Second, the *sec18* block represents the first known postinternalization block in endocytosis. This was concluded from the following experiments. When α-factor was internalized in the *sec12* mutant, it accumulated in biochemically defined early endosomes

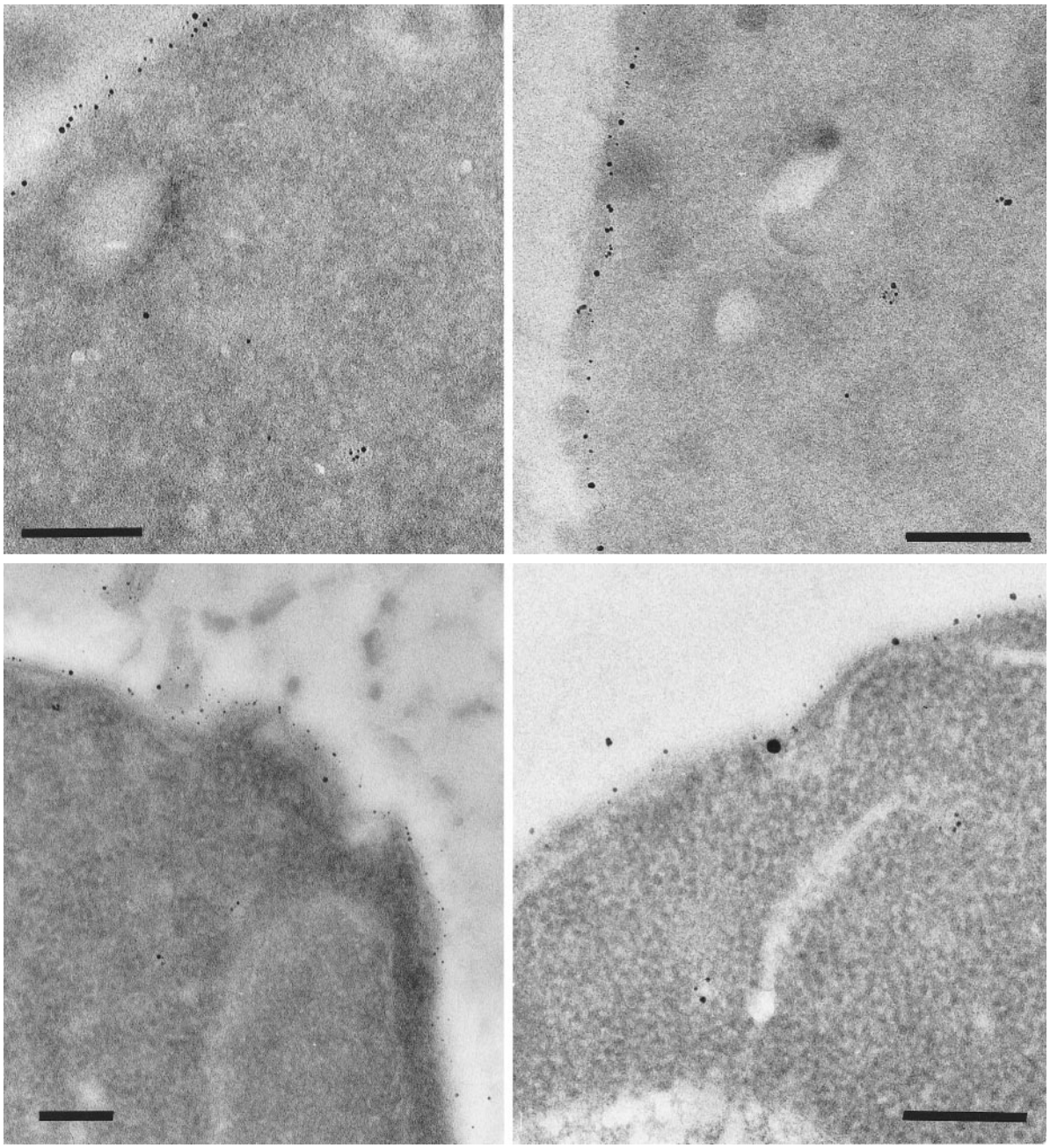

Figure 11. Putative primary endocytic vesicle profiles. Profiles of putative primary endocytic vesicles were taken from *sec18* spheroplasts incubated for 30 min at 32°C with positively charged Nanogold.

(Hicke *et al.*, 1997). Detection of the α-factor receptor by immunofluorescence under similar conditions in *sec12* cells revealed that the receptor was concentrated in peripheral, relatively large punctate structures. Similar experiments using the *sec18* mutant showed accumulation of the α-factor receptor in smaller, peripheral dots by immunofluorescence easily distinguishable from the structures accumulated in *sec12* cells. A double mutant (*sec12 sec18*) showed a *sec18* phenotype. These data showed that the small, peripheral dots that accumulated in *sec18* cells were epistatic to and preceded the large peripheral compartment, which fractionated like the biochemically defined early endosomes. The small peripheral dots seen in *sec18* cells, therefore, are likely precursors of the early endosomes seen by immunofluorescence in *sec12* cells

and must correspond to the vesicles seen here in *sec18* spheroplasts because they contain all of the internalized label. Third, mammalian Sec18p has been shown to associate with endocytic clathrin- coated vesicles, and N-ethylmaleimide, an inhibitor of Sec18p, blocks fusion of clathrin-coated vesicles (Woodman and Warren, 1991; Steel *et al.*, 1996). Finally, the vesicles seen in *sec18* spheroplasts resemble the first endocytic intermediates observed using wild-type spheroplasts at 15°C.

The molecular requirements for the internalization step of endocytosis in yeast show similarities to several different types of endocytic internalization seen in mammalian cells, but the similarities are not close enough to any of them to be certain of a true homology in mechanism (Riezman *et al.*, 1996). For instance, mutations in clathrin affect the internalization of ligands in both cell types, but in yeast this effect is only partial. On the other hand, actin is absolutely required for endocytosis in yeast, whereas actin depolymerization in animal cells using cytochalasin D has been proposed to affect clathrin-dependent internalization from apical, but not basolateral, plasma membrane (Gottlieb *et al.*, 1993; Jackman *et al.*, 1994). This does not rule out that actin is required for clathrin-mediated endocytosis at the basolateral surface because cytochalasin D may not depolymerize all cellular actin equally. In fact, a role for actin in all clathrin-mediated endocytosis has been proposed recently (Lamaze *et al.*, 1997). Actin is also required for two other types of endocytic internalization in animal cells: induced internalization through caveolae (Parton *et al.*, 1994) and phagocytosis (Greenberg *et al.*, 1991). A clear distinction between the clathrin or caveolar uptake and phagocytic uptake is the size of the primary endocytic vesicles. For this reason it was important to identify the primary endocytic vesicle in yeast.

The size and regularity of the putative primary endocytic vesicles described here would be most consistent with their being derived through a coat-dependent mechanism, rather than a solely actin-based, phagocytic-like mechanism. The size of the primary endocytic structure determined by the latter mechanism depends upon the size of the particle being internalized, not upon the dimensions of an assembled coat structure, such as clathrin coats or caveolar coats. It is hard to imagine how actin could generate small, uniform vesicles independent of a coat protein. In yeast, no protein with clear sequence homology to caveolin is present; therefore, a caveolin homologue apparently plays no role in this event. On the other hand, clathrin coats could participate in endocytic internalization because clathrin mutants show a 50% block in this step. One possible role for clathrin in endocytosis that would be consistent with the partial block could be the regulation of the size of the endocytic vesicle and/or the recruitment of receptors into internalization structures. The precise role of clathrin in the process of internalization will have to await further experimentation and would benefit greatly from the detection of the internalization structures. Hopefully, some of the *end* mutants that affect the internalization step of endocytosis will be useful for this.

ACKNOWLEDGMENTS

We thank Richard W. Burry for helpful advice, the members of the Interdepartmental EM of the Biozentrum for their help, and Kathleen D'Hondt, M. Isabel Geli, and Andreas Wesp for critical reading of the manuscript. This work was supported by the Canton of Basel-Stadt and by grants from the Swiss National Science Foundation (to H.R.).

REFERENCES

Bénédetti, H., Raths, S., Crausaz, F., and Riezman, H. (1994). The END3 gene encodes a protein that is required for the internalization step of endocytosis and for actin cytoskeleton organization in yeast. Mol. Biol. Cell *5*, 1023–1037.

Benmerah, A., Gagnon, J., Begue, B., Megarbane, B., Dautry-Varsat, A., and Cerf-Bensussan, B.N. (1995). The tyrosine kinase substrate eps15 is constitutively associated with the plasma membrane adaptor AP-2. J. Cell Biol. *131*, 1831–1838.

Berkower, C., Loayza, D., and Michaelis, S. (1994). Metabolic instability and constitutive endocytosis of STE6, the a-factor transporter of *Saccharomyces cerevisiae*. Mol. Biol. Cell *5*, 1185–1198.

Davis, N.G., Horecka, J.L., and Sprague, G.F., Jr. (1993). Cis- and trans-acting functions required for endocytosis of the yeast pheromone receptors. J. Cell Biol. *122*, 53–65.

Dulic, V., Egerton, M., Elguindi, I., Raths, S., Singer, B., and Riezman, H. (1991). Yeast endocytosis assays. Methods Enzymol. *194*, 697–710.

Egner, R., Mahe, Y., Pandjaitan, R., and Küchler, K. (1995). Endocytosis and vacuolar degradation of the plasma membrane-localized Pdr5 ATP-binding cassette multidrug transporter in *Saccharomyces cerevisiae*. Mol. Cell. Biol. *15*, 5879–5887.

Galan, J.M., Moreau, V., André, B., Volland, C., and Haguenauer-Tsapis, R. (1996). Ubiquitination mediated by the Npi1p/Rsp5p ubiquitin-protein ligase is required for endocytosis of the yeast uracil permease. J. Biol. Chem. *271*, 10946–10952.

Geli, M.I., and Riezman, H. (1996). Role of type I myosins in receptor-mediated endocytosis in yeast. Science *272*, 533–535.

Gorvel, J.P., Chavrier, P., Zerial, M., and Gruenberg, J. (1991). rab5 controls early endosome fusion in vitro. Cell *64*, 915–925.

Gottlieb, T.A., Ivanov, I.E., Adesnik, M., and Sabatini, D.D. (1993). Actin microfilaments play a critical role in endocytosis at the apical but not the basolateral surface of polarized epithelial cells. J. Cell Biol. *120*, 695–710.

Graham, T.R., and Emr, S.D. (1991). Compartmental organization of Golgi-specific protein modification and vacuolar protein sorting events defined in a yeast sec18 (NSF) mutant. J. Cell Biol. *114*, 207–218.

Greenberg, S., el Khoury, J., di Virgilio, F., Kaplan, E.M., and Silverstein, S.C. (1991). Ca(2+)-independent F-actin assembly and disassembly during Fc receptor-mediated phagocytosis in mouse macrophages. J. Cell Biol. *113*, 757–767.

Haas, A., and Wickner, W. (1996). Homotypic vacuole fusion requires Sec17p (yeast alpha-SNAP) and Sec18p (yeast NSF). EMBO J. *15*, 3296–3305.

Hein, C., Springael, J.Y., Volland, C., Haguenauer-Tsapis, R., and André, B. (1995). NPI1, an essential yeast gene involved in induced degradation of Gap1 and Fur4 permeases, encodes the Rsp5 ubiquitin-protein ligase. Mol. Microbiol. *18*, 77–87.

Hicke, L., and Riezman, H. (1996). Ubiquitination of a yeast plasma membrane receptor signals its ligand-stimulated endocytosis. Cell *84*, 277–287.

Hicke, L., Zanolari, B., Pypaert, M., Rohrer, J., and Riezman, H. (1997). Transport through the yeast endocytic pathway occurs through morphologically distinct compartments and requires an active secretory pathway and Sec18p/N-ethylmaleimide-sensitive fusion protein. Mol. Biol. Cell *8*, 13–31.

Hopkins, C.R., Gibson, A., Shipman, M., and Miller, K. (1990). Movement of internalized ligand-receptor complexes along a continuous endosomal reticulum. Nature *346*, 335–339.

Jackman, M.R., Shurety, W., Ellis, J.A., and Luzio, J.P. (1994). Inhibition of apical but not basolateral endocytosis of ricin and folate in Caco-2 cells by cytochalasin D. J. Cell Sci. *107*, 2547–2556.

Kaiser, C.A., and Schekman, R. (1990). Distinct sets of SEC genes govern transport vesicle formation and fusion early in the secretory pathway. Cell *61*, 723–733.

Kübler, E., and Riezman, H. (1993). Actin and fimbrin are required for the internalization step of endocytosis in yeast. EMBO J. *12*, 2855–2862.

Kübler, E., Schimmöller, F., and Riezman, H. (1994). Calcium-independent calmodulin requirement for endocytosis in yeast. EMBO J. *13*, 5539–5546.

Lai, K., Bolognese, C.P., Swift, S., and McGraw, P. (1995). Regulation of inositol transport in *Saccharomyces cerevisiae* involves inositol-induced changes in permease stability and endocytic degradation in the vacuole. J. Biol. Chem. *270*, 2525–2534.

Lamaze, C., Fujimoto, L.M., Yin, H.L., and Schmid, S.L. (1997). The actin cytoskeleton is required for receptor-mediated endocytosis in mammalian cells. J. Biol. Chem. *272*, 20332–20335.

McDowall, A., Gruenberg, J., Römisch, K., and Griffiths, G. (1989). The structure of organelles of the endocytic pathway in hydrated cryosections of cultured cells. Eur. J. Cell Biol. *49*, 281–294.

Munn, A.L., and Riezman, H. (1994). Endocytosis is required for the growth of vacuolar H(+)-ATPase-defective yeast: identification of six new END genes. J. Cell Biol. *127*, 373–386.

Munn, A.L., Stevenson, B.J., Geli, M.I., and Riezman, H. (1995). end5, end6, and end7: mutations that cause actin delocalization and block the internalization step of endocytosis in *Saccharomyces cerevisiae*. Mol. Biol. Cell *6*, 1721–1742.

Parton, R.G., Joggerst, B., and Simons, K. (1994). Regulated internalization of caveolae. J. Cell Biol. *127*, 1199–1215.

Raths, S., Rohrer, J., Crausaz, F., and Riezman, H. (1993). end3 and end4: two mutants defective in receptor-mediated and fluid- phase endocytosis in *Saccharomyces cerevisiae*. J. Cell Biol. *120*, 55–65.

Riezman, H. (1985). Endocytosis in yeast: several of the yeast secretory mutants are defective in endocytosis. Cell *40*, 1001–1009.

Riezman, H. (1993). Yeast endocytosis. Trends Cell Biol. *3*, 273–277.

Riezman, H., Munn, A., Geli, M.I., and Hicke, L. (1996). Actin-, myosin- and ubiquitin-dependent endocytosis. Experientia *52*, 1033–1041.

Schandel, K.A., and Jenness, D.D. (1994). Direct evidence for ligand-induced internalization of the yeast alpha-factor pheromone receptor. Mol. Cell. Biol. *14*, 7245–7255.

Schimmöller, F., and Riezman, H. (1993). Involvement of Ypt7p, a small GTPase, in traffic from late endosome to the vacuole in yeast. J. Cell Sci. *106*, 823–830.

Shupliakov, O., Löw, P., Grabs, D., Gad, H., Chen, H., David, C., Takei, K., de Camilli, P., and Brodin, L. (1997). Synaptic vesicle endocytosis impaired by disruption of dynamin-SH3 domain interactions. Science *276*, 259–263.

Singer, B., and Riezman, H. (1990). Detection of an intermediate compartment involved in transport of alpha-factor from the plasma membrane to the vacuole in yeast. J. Cell Biol. *110*, 1911–1922.

Singer-Krüger, B., Frank, R., Crausaz, F., and Riezman, H. (1993). Partial purification and characterization of early and late endosomes from yeast. Identification of four novel proteins. J. Biol. Chem. *268*, 14376–14386.

Singer-Krüger, B., Stenmark, H., and Zerial, M. (1995). Yeast Ypt51p and mammalian Rab5: counterparts with similar function in the early endocytic pathway. J. Cell Sci. *108*, 3509–3521.

Sivadon, P., Bauer, F., Aigle, M., and Crouzet, M. (1995). Actin cytoskeleton and budding pattern are altered in the yeast rvs161 mutant: the Rvs161 protein shares common domains with the brain protein amphiphysin. Mol. Gen. Genet. *246*, 485–495.

Staub, O., Dho, S., Henry, P., Correa, J., Ishikawa, T., McGlade, J., and Rotin, D. (1996). WW domains of Nedd4 bind to the proline-rich PY motifs in the epithelial Na+ channel deleted in Liddle's syndrome. EMBO J. *15*, 2371–2380.

Steel, G.J., Tagaya, M., and Woodman, P.G. (1996). Association of the fusion protein NSF with clathrin-coated vesicle membranes. EMBO J. *15*, 745–752.

Stoorvogel, W., Oorschot, V., and Geuze, H.J. (1996). A novel class of clathrin-coated vesicles budding from endosomes. J. Cell Biol. *132*, 21–33.

Strous, G., van Kerkof, P., Govers, R., Ciechanover, A., and Schwartz, A.L. (1996). The ubiquitin conjugation system is required for ligand-induced endocytosis and degradation of the growth hormone receptor. EMBO J. *15*, 3806–3812.

Tan, P.K., Davis, N.G., Sprague, G.F., and Payne, G.S. (1993). Clathrin facilitates the internalization of seven transmembrane segment receptors for mating pheromones in yeast. J. Cell Biol. *123*, 1707–1716.

Tebar, F., Sorkina, T., Sorkin, A., Ericsson, M., and Kirchhausen, T. (1996). Eps15 is a component of clathrin-coated pits and vesicles and is located at the rim of coated pits. J. Biol. Chem. *271*, 28727–28730.

van Tuinen, E. and Riezman, H. (1987). Immunolocalization of glyceraldehyde-3-phosphate dehydrogenase, hexokinase, and carboxypeptidase Y in yeast cells at the ultrastructural level. J. Histochem. Cytochem. *35*, 327–333.

Vida, T.A., and Emr, S.D. (1995). A new vital stain for visualizing vacuolar membrane dynamics and endocytosis in yeast. J. Cell Biol. *128*, 779–792.

Volland, C., Urban-Grimal, D., Geraud, G., and Haguenauer-Tsapis, R. (1994). Endocytosis and degradation of the yeast uracil permease under adverse conditions. J. Biol. Chem. *269*, 9833–9841.

Wendland, B., McCaffery, J.M., Xiao, Q., and Emr, S.D. (1996). A novel fluorescence-activated cell sorter-based screen for yeast endocytosis mutants identifies a yeast homologue of mammalian eps15. J. Cell Biol. *135*, 1485–1500.

Wong, W.T., Schumacher, C., Salcini, A.E., Romano, A., Castagnino, P., Pelicci, P.G., and Di Fiore, P. (1995). A protein-binding domain, EH, identified in the receptor tyrosine kinase substrate Eps15 and conserved in evolution. Proc. Natl. Acad. Sci. USA *92*, 9530–9534.

Woodman, P.G., and Warren, G. (1991). Isolation of functional, coated, endocytic vesicles. J. Cell Biol. *112*, 1133–1141.